Framework for Probabilistic Assessment of Maximum Nonlinear Structural Response Based on Sensor Measurements: Discretization and Estimation

Ajay Saini, S.M.ASCE[1]; and Iris Tien, Ph.D., A.M.ASCE[2]

Abstract: A probabilistic framework to draw real-time inferences on the maximum response of an uncertain nonlinear structural system under stochastic excitation based on sensor measurements is proposed. The primary contributions are twofold: first, an exact discretization solution is derived for the system evolution equation for the nonlinear case. This is validated against a Taylor expansion discretization solution. Second, a methodology for robust Bayesian estimation of the time-evolving system state is proposed. The system is instrumented by sensors placed on the structure with inferences drawn using Kalman-based approaches. The sensor observations are used in real time to estimate system state without any knowledge of the time history of the input motion. The distribution of the maximum response is assessed. The proposed methodology is applied to a 10-story shear-type sample structure under earthquake loading. The interstory drift is analyzed with measured data collected through accelerometers placed on the building. A simulation approach is used to demonstrate the ability of the proposed methodology to accurately estimate nonlinear structural response based on sensor measurements. In addition, the method is shown to be robust to varying system characteristics. This includes uncertainties in the structural, ground, and input motion parameters, as well as varying measurement characteristics. **DOI:** [10.1061/(ASCE)EM.1943-7889.0001277](#). © 2017 American Society of Civil Engineers.

Introduction

Inferring the response of a structure is an important task in structural reliability assessment and structural health monitoring, and it is beneficial to be able to do so based on information from simple, noninvasive sensor measurements, e.g., from accelerometers placed sparsely on the structure. With the growing inclusion of nonlinear behavior of a structure in design and analysis, the ability to assess nonlinear structural response is becoming increasingly valuable. A probabilistic approach is required because of uncertainties in both sensor measurements, e.g., with noisy data, and inputs, e.g., under stochastic loadings. Such systems, which are also evolving with time, are effectively visualized as a dynamic Bayesian network (DBN) with states estimated using Kalman-based approaches. In this study, the focus is on real-time processing of the data from accelerometers mounted on the structure to infer the maximum structural response, including maximum interstory drift, when the structure is subjected to unknown stochastic excitations.

Previously, Tien et al. (2016) proposed a probabilistic framework to infer structural response in the linear range based on accelerometer data. However, the methodology changes considerably for nonlinear behavior. The dynamic data in such nonlinear systems can be processed using frameworks such as the extended Kalman filter (EKF) and unscented Kalman filter (UKF). The EKF and the UKF are able to use the data measured by accelerometers to estimate the structural response, including displacement-based responses, without any prior knowledge of the excitation, e.g., an earthquake ground motion. This also requires a discretization solution for the continuous system.

The study begins with an observation matrix of structural accelerations due to a random earthquake input, including terms for measurement error and ambient noise. Using Kalman estimation methods, the output of the DBN is inference on the mean displacements and velocities at each time step of the data recording and the time-evolving joint probability distribution of the displacement and velocity responses. This is used in estimating a stochastic distribution of the maximum response. The study demonstrates the ability of the methodology in the nonlinear case to estimate the displacement response from accelerometer measurements and obtain analytical probabilistic distributions of the maximum response exceeding desired response levels for high thresholds. This estimation is shown to be robust to various system uncertainties.

The rest of the paper is organized as follows. The following section provides background on related work in this area. Next, the proposed framework is described. This includes descriptions of the structural and ground dynamical subsystems, and the derived discretization solution for the continuous system. The methodology for estimating the system state and the distribution of the maximum response is described. The proposed method is then applied to the case of a multistory shear-type building model under seismic excitation. Several inference results from this example case are presented, including: comparisons of the two formulations, EKF and UKF; stochastic distributions of interstory drifts; distributions of the maximum structural response; and the effects of parameter uncertainties and varying measurement characteristics on the estimation results. The proposed framework supports structural reliability assessment and decision making for structural health monitoring applications, including the design of effective instrumentation strategies. It provides a basis for the use of accelerometer readings even under conditions of uncertainty to estimate nonlinear structural response.

[1]Ph.D. Candidate, School of Civil and Environmental Engineering, Georgia Institute of Technology, 790 Atlantic Dr., Atlanta, GA 30332-0355 (corresponding author). ORCID: http://orcid.org/0000-0002-7882-278X. E-mail: ajaysaini@gatech.edu

[2]Assistant Professor, School of Civil and Environmental Engineering, Georgia Institute of Technology, 790 Atlantic Dr., Atlanta, GA 30332-0355. E-mail: itien@ce.gatech.edu

Background and Related Work

The dynamic Bayesian network is a probabilistic framework that models the evolution of a system over time. It is comprised of a sequence of Bayesian networks (BNs) connected by direct links to advance the system at each time step based on the prior information. The reader is referred to Murphy (2002, 2012) and Barber (2012) for an overview of DBNs. Bayesian models have previously been used in various civil and structural engineering applications. This includes work in structural health monitoring to probabilistically measure damage such as Vanik and Beck (1997) and Vanik et al. (2000); work in structural model updating such as Katafygiotis and Yuen (2001), Yuen and Katafygiotis (2002), and Au et al. (2013); and work in system-level reliability assessment such as Tien (2014) and Zhang and Au (2015). In contrast to these previous studies, the goal of this study is to estimate the nonlinear structural response, including displacement-based interstory drifts, based solely on sensor measurements without knowledge of the excitation time history.

To do this, the extended Kalman filter and unscented Kalman filter are used. The EKF and the UKF have been developed to estimate the system state for a dynamically evolving nonlinear system. These two methods can be used to perform computations over the DBN to obtain the marginal system state at every time step and project the trajectory of the evolving system. The reader is referred to texts such as Kalman (1960) and Terejanu (2008) for detailed descriptions of the Kalman, EKF, and UKF models. In the past, EKF and UKF have been used most widely in nonlinear analysis for system identification as in Hoshiya and Saito (1984), Jeen-Shang and Yigong (1994), and more recently in Al-Hussein and Haldar (2015), and Mu and Yuen (2015); and to identify structural damage through structural parameter approximation as in Yang et al. (2006, 2007). The UKF has been used in dynamical structural engineering applications in Mariani and Ghisi (2007) and for real-time nonlinear structural system identification in Wu and Smith (2007), Chatzi and Smyth (2009), and Xie and Feng (2012).

In these studies, known excitations are used to identify or update the structural parameters. However, in this study the excitation is unknown and structural system parameters are assumed to be estimated beforehand. Without knowledge of the ground motion time history, e.g., the accelerogram of the earthquake, the goal is to use only the sensor observations, e.g., from structure-mounted accelerometers, to estimate the system state in real time. The effect of uncertainty or errors in the initial estimation of the structural parameters is investigated later in the study.

In addition, the methodology presented in this paper requires discretization of the continuous dynamical equation of motion, which may not be readily integrable. An exact discretization solution is derived for the equation of motion satisfying a Lagrange partial differential equation (PDE) condition. Lagrange methods for discretization of nonlinear engineering problems have previously been used in control systems as in Hori et al. (1992), Markazi and Hori (1995), and Nesic and Teel (2004); mathematical applications such as Guy (2006); and systems with exact discretization solutions such as Sakamoto et al. (2011). The solution described in this paper is specifically for structural response evolution. The exact solution is compared to a second discretization solution derived based on the Taylor expansion. This method of discretization of nonlinear systems has been used for approximate solutions in engineering applications, (e.g., Kazantzis and Kravaris 1999; Zhang and Chong 2006; Zhang et al. 2011; Zheng et al. 2013).

To describe the system nonlinearity, the Bouc-Wen model proposed in Bouc (1967) and Wen (1976) is used in this study. This model has been widely used in nonlinear structural analysis as in Wen (1980), Wen (1989), Hurtado and Barbat (1996), Song and Der Kiureghain (2006), and Ikhouane et al. (2007). In addition to real-time estimation of the structural response, this study is also interested in a probabilistic distribution of the maximum response. To obtain this, the probability of up-crossings of a nonstationary process as initially formulated by Rice (1944) and subsequently derived for non-zero-mean processes in Tien et al. (2016) is used. This employs an approximation of the crossings of the maximum structural response over a safe threshold as Poisson events. Finally, while the methodology is applicable to any stochastic excitation, this study assesses the response of the structure to a seismic excitation in particular. To do this, accelerometer observations under a random earthquake are simulated. The simulation of ground motion is performed as in Rezaeian and Der Kiureghian (2010). The choice of parameters in the model of the ground excitation is described in the "Application" section of this paper.

Methodology

The proposed framework consists of two major sections: discretization solution and state estimation. The equation of motion is a second order differential equation while the recorded sensor data is discretized. Therefore, a discretization solution is needed to process the data.

Discretization

The dynamical system is modeled as a cascade of two dynamical subsystems. First, the ground dynamical subsystem takes white noise at the bedrock as input and produces an acceleration at the surface. Second, the structural subsystem takes the input ground surface acceleration and produces the output structural response. In this formulation, a capital bold letter (e.g., $\mathbf{M}$) represents a matrix, a small bold letter (e.g., $\mathbf{u_s}$) represents a vector and a small italic letter (e.g., a_g) represents a scalar quantity. The letter $\mathbf{u}$ represents displacement while a represents acceleration, and subscripts s and g indicate variables for the structure and ground, respectively.

Structural Dynamical Subsystem
In the structural subsystem, nonlinearity may be caused by nonlinear stiffness or damping. The earthquake-induced forces also cause nonlinearity due to P-δ and P-Δ effects. In this study, approximate amplification factor B_2 is used for force nonlinearity, as specified per Appendix 8 of the AISC Steel Construction Manual and calculated using approximate second-order analysis. Nonlinear behavior of a steel structure is considered for this study. However, the methodology may be used for nonlinearity of any structural material.

The equation of motion for the structure subjected to base motion is given by

$$\mathbf{M\ddot{u}_s} + \mathbf{C\dot{u}_s} + \mathbf{F(u_s)} = -B_2\mathbf{M1}a_g + \mathbf{f} \qquad (1)$$

where $\mathbf{M}$, $\mathbf{C}$ and $\mathbf{F}$ represent the mass, damping, and spring force matrices, respectively; and $\mathbf{f}$ represents ambient vibrations and additional uncertainty in the external force during the seismic event. Defining $\mathbf{z_s^T} := \begin{bmatrix} \mathbf{u_s^T} & \mathbf{\dot{u}_s^T} \end{bmatrix}$ in first-order form, the equation of motion is

$$\mathbf{\dot{z}_s} = \begin{bmatrix} \mathbf{0} & \mathbf{I} \\ \mathbf{0} & -\mathbf{M^{-1}C} \end{bmatrix} \mathbf{z_s} + \begin{bmatrix} \mathbf{0} \\ -\mathbf{M^{-1}F(z_s)} \end{bmatrix} + \begin{bmatrix} \mathbf{0} \\ -\mathbf{1} \end{bmatrix} B_2 a_g + \begin{bmatrix} \mathbf{0} \\ \mathbf{M^{-1}} \end{bmatrix} \mathbf{f}$$

$$(2)$$

where B_2 is defined from AISC specification Appendix 8 as

$$B_2 := \frac{1}{1 - \frac{P_{story}}{P_{estory}}} \tag{3}$$

$$P_{estory} := 0.85 \frac{HL}{\Delta h} \tag{4}$$

where H = total horizontal force at the degree of freedom; L = height of the story; P_{story} = total vertical load supported by the story; and Δh = first order deflection due to H and L.

Ground Dynamical Subsystem

The equation of motion for the ground surface with respect to the bedrock-modulated white noise w is given by

$$\ddot{u}_g + 2\xi_g\omega_g\dot{u}_g + \omega_g^2 u_g = -w \tag{5}$$

where the frequency and damping ratio of the ground filter are represented by ω_g and ξ_g, respectively. Defining $\mathbf{z_g} := [\, u_g \quad \dot{u}_g \,]^T$, the equation of motion in first-order form is

$$\dot{\mathbf{z}}_\mathbf{g} = \begin{bmatrix} 0 & 1 \\ -\omega_g^2 & -2\xi_g\omega_g \end{bmatrix} \mathbf{z_g} + \begin{bmatrix} 0 \\ -1 \end{bmatrix} w \tag{6}$$

The total acceleration at the surface of ground, a_g, is given as

$$a_g = \ddot{u}_g + w = [\, -\omega_g^2 \quad -2\xi_g\omega_g \,]\mathbf{z_g} \tag{7}$$

State Space Representation

Combining the two subsystems in first-order form and defining $\mathbf{z}^T := [\, \mathbf{z_g^T} \quad \mathbf{z_s^T} \,]$ yields the state space representation of the dynamic system as

$$\dot{\mathbf{z}} = \begin{bmatrix} 0 & 1 & \mathbf{0} & \mathbf{0} \\ -\omega_g^2 & -2\xi_g\omega_g & \mathbf{0} & \mathbf{0} \\ \mathbf{0} & \mathbf{0} & \mathbf{0} & \mathbf{I} \\ 1B_2\omega_g^2 & 12B_2\xi_g\omega_g & \mathbf{0} & -\mathbf{M^{-1}C} \end{bmatrix} \mathbf{z} + \begin{bmatrix} 0 \\ 0 \\ \mathbf{0} \\ -\mathbf{M^{-1}F(z_s)} \end{bmatrix}$$
$$+ \begin{bmatrix} 0 \\ -1 \\ \mathbf{0} \\ \mathbf{0} \end{bmatrix} w + \begin{bmatrix} 0 \\ 0 \\ \mathbf{0} \\ \mathbf{M^{-1}} \end{bmatrix} \mathbf{f} \tag{8}$$

$$\dot{\mathbf{z}} = \mathbf{A_c(z)} + \mathbf{b_c}w + \mathbf{B_c f} \tag{9}$$

Discretization Solution: Exact

Next, the continuous system must be discretized in the time domain. A direct integration of the differential form given in Eq. (10) cannot be used as the nonlinearity is because of one element of the vector $\mathbf{z}$ and occurs nonuniformly in Eq. (9)

$$\int_{\mathbf{z_k}}^{\mathbf{z_{k+1}}} \frac{d\mathbf{z}}{\mathbf{A_c(z)z} + \mathbf{b_c}w + \mathbf{B_c f}} = \int_t^{t+\Delta t} dt \tag{10}$$

Therefore, a discretization solution is derived. This exact solution is later verified using a Taylor expansion-based discretization. For the exact solution, the given system, $\dot{\mathbf{z}} = \mathbf{A_c(z)z} + \mathbf{b_c}w + \mathbf{B_c f}$, is transformed into a linear system, $d\mathbf{y}/dt = \mathbf{y}(t)$, using a transformation to the differential form $\mathbf{y} = \exp(\mathbf{V(z)})\mathbf{1}$, where $\mathbf{V(z)}$ is a $n \times n$ matrix as in Sakamoto et al. (2011).

Defining $\mathbf{z} = [\, \mathbf{z_1} \quad \mathbf{z_2} \quad \mathbf{z_3} \quad \mathbf{z_4} \,]$, linearization is possible if the following condition is satisfied:

$$\mathbf{f}_1(z,t)\frac{\partial \mathbf{V}(z,t)}{\partial z_1} + \ldots + \mathbf{f}_4(z,t)\frac{\partial \mathbf{V}(z,t)}{\partial z_4} = \mathbf{I}_n \tag{11}$$

The four governing equations are

$$\dot{z}_1 = \mathbf{f}_1(\mathbf{z},t) = z_2 \tag{12}$$

$$\dot{z}_2 = \mathbf{f}_2(\mathbf{z},t) = -\omega_g^2 z_1 - 2\xi_g\omega_g z_2 - w \tag{13}$$

$$\dot{z}_3 = \mathbf{f}_3(\mathbf{z},t) = z_4 \tag{14}$$

$$\dot{z}_4 = \mathbf{f}_4(\mathbf{z},t)$$
$$= 1B_2\omega_g^2 z_1 + 12B_2\xi_g\omega_g z_2 - \mathbf{M^{-1}F(z_3)} - \mathbf{M^{-1}Cz_4} + \mathbf{M^{-1}f} \tag{15}$$

Unless the damping is nonlinear, the previous partial differential equations are linear with respect to their corresponding elements. The treatment for the case of nonlinear damping is described later in this section.

For linearized equations, Lagrange characteristic equations per Eq. (11) can be written as

$$\mathbf{f_j}(z,t)\frac{\partial \mathbf{V}(z,t)}{\partial z_j} = \mathbf{I_j} \qquad j \in [1,4] \tag{16}$$

Solution of the characteristic equations results in the values of the elements of $\mathbf{V}$.

Given $\int dy/y(t) = \int dt$ and the transformation for $\mathbf{y}$, this yields $[\ln(\mathbf{y})]_k^{k+1} = \int dt$ and

$$[(\mathbf{V(z)}\mathbf{1})]_k^{k+1} = \mathbf{I} \int dt \tag{17}$$

Using Eqs. (12)–(15) and Eq. (16) together, the authors obtain for the elements of $\mathbf{V}$

$$[\mathbf{V_{11}}]_k^{k+1} z_{2_k} = \int_{z_{1_k}}^{z_{1_{k+1}}} dz_1 = z_{1_{k+1}} - z_{1_k} \tag{18}$$

$$[\mathbf{V_{22}}]_k^{k+1}$$
$$= \frac{\ln(-\omega_g^2 z_{1_k} - 2\xi_g\omega_g z_{2_{k+1}} - w_k) - \ln(-\omega_g^2 z_{1_k} - 2\xi_g\omega_g z_{2_k} - w_k)}{-2\xi_g\omega_g} \tag{19}$$

$$[\mathbf{V_{33}}]_k^{k+1} \mathbf{z_{4_k}} = \mathbf{z_{3_{k+1}}} - \mathbf{z_{3_k}} \tag{20}$$

$$[\mathbf{V_{44}}]_k^{k+1}$$
$$= \text{inv}(-\mathbf{M^{-1}C})\big(\ln(1B_2\omega_g^2 z_{1k} + 12B_2\xi_g\omega_g z_{2k} - \mathbf{M^{-1}F(z_{3_k})} - \mathbf{M^{-1}Cz_{4_{k+1}}} - \mathbf{M^{-1}f_k})$$
$$- \ln(1B_2\omega_g^2 z_{1k} + 12B_2\xi_g\omega_g z_{2k} - \mathbf{M^{-1}F(z_{3_k})} - \mathbf{M^{-1}Cz_{4_k}} - \mathbf{M^{-1}f_k})\big) \tag{21}$$

While nonlinear stiffness is treated in this study, if damping coefficient C is nonlinear, it can be integrated into Eq. (15) according to the nonlinear function. For this study, using Eq. (17) and Eqs. (18)–(21) together, the following system evolution equations are obtained in discrete time with Δt indicating the discretization time step

$$z_{1_{k+1}} = z_{1_k} + z_{2_k}\Delta t \tag{22}$$

$$z_{2_{k+1}} = \frac{[(-\omega_g^2 z_{1_k} - 2\xi_g\omega_g z_{2_k} - w_k)\exp(-2\xi_g\omega_g\Delta t)] + w_k + \omega_g^2 z_{1_k}}{-2\xi_g\omega_g} \tag{23}$$

$$\mathbf{z}_{3_{k+1}} = \mathbf{z}_{3_k} + \mathbf{z}_{4_k}\Delta t \tag{24}$$

$$\begin{aligned}
\mathbf{z}_{4_{k+1}} = (-\mathbf{MC}^{-1})[\{(1B_2\omega_g^2 z_1 + 12B_2\xi_g\omega_g z_2 - \mathbf{M}^{-1}\mathbf{F}(\mathbf{z}_{3_k}) \\
- \mathbf{M}^{-1}\mathbf{C}\mathbf{z}_{4_k} - \mathbf{M}^{-1}\mathbf{f_k})e^{-\mathbf{M}^{-1}\mathbf{C}\Delta t}\} \\
- (-1B_2\omega_g^2 z_1 - 12B_2\xi_g\omega_g z_2 + \mathbf{M}^{-1}\mathbf{F}(\mathbf{z}_{3_k}) + \mathbf{M}^{-1}\mathbf{f_k})] \tag{25}
\end{aligned}$$

In matrix form, this can be written as

$$\mathbf{z}_{k+1} = \mathbf{A}_1\mathbf{z}_k + \mathbf{F}_1 + \mathbf{b}w_k + \mathbf{B}\mathbf{f}_k \tag{26}$$

where

$$\mathbf{A}_1 = \begin{bmatrix} 1 & \Delta t & \mathbf{0} & \mathbf{0} \\ \dfrac{-\omega_g^2(e^{-2\xi_g\omega_g\Delta t}-1)}{-2\xi_g\omega_g} & e^{-2\xi_g\omega_g\Delta t} & \mathbf{0} & \mathbf{0} \\ \mathbf{0} & \mathbf{0} & \mathbf{I} & \mathbf{I}\Delta t \\ B_2\omega_g^2(-\mathbf{MC}^{-1})(e^{-\mathbf{M}^{-1}\mathbf{C}\Delta t}-\mathbf{I}) & 2B_2\xi_g\omega_g(-\mathbf{MC}^{-1})(e^{-\mathbf{M}^{-1}\mathbf{C}\Delta t}-\mathbf{I}) & \mathbf{0} & e^{-\mathbf{M}^{-1}\mathbf{C}\Delta t} \end{bmatrix} \tag{27}$$

$$\mathbf{F}_1 = \begin{bmatrix} 0 \\ 0 \\ \mathbf{0} \\ \mathbf{C}^{-1}(e^{-\mathbf{M}^{-1}\mathbf{C}\Delta t}-1)\mathbf{F}(z_s) \end{bmatrix} \tag{28}$$

$$\mathbf{b} = \frac{\mathbf{b}_c(e^{-2\xi_g\omega_g\Delta t}-1)}{-2\xi_g\omega_g} \tag{29}$$

$$\mathbf{B} = (-\mathbf{MC}^{-1})(e^{-\mathbf{M}^{-1}\mathbf{C}\Delta t}-\mathbf{I})\mathbf{B}_c \tag{30}$$

This process yields the exact discretization result for the nonlinear equations modeling the structural response. The accuracy of this solution is only dependent on the discretization step, i.e., the sampling period of the sensor. The method is exact for all other parameters.

Discretization Solution: Taylor Expansion
A discretization solution based on an infinite Taylor series expansion of the equation is now provided. This is used to verify the exact solution presented in the previous section. Consider a nonlinear dynamic system with state space given as

$$\dot{\mathbf{z}} = f(\mathbf{z}) + pg(\mathbf{z}) \tag{31}$$

where $\mathbf{z}$ = state variable; p = scalar input; and f and g = smooth functions of $\mathbf{z}$. For such a case, the Taylor method for discretization can be used to obtain an approximate solution as in Kazantis and Kravaris (1999). The solution begins with a uniformly convergent Taylor series with coefficients given as functions of successive partial derivatives such that

$$\mathbf{z}_{k+1} = \mathbf{z}_k + \sum_{l=1}^{\infty} \frac{T^l}{l!}\frac{d^l\mathbf{z}}{dt^l}\bigg|_{t_k} \tag{32}$$

where $T = t_{k+1} - t_k$ is the sampling period; and $\mathbf{z}(k)$ = state space vector at time $t_k = kT$. Eq. (32) can be written as

$$z_{k+1} = z_k + \sum_{l=1}^{\infty} A^{[l]}(z_k, p_k)\frac{T^l}{l!} \tag{33}$$

where $A^{[1]}(\mathbf{z},w) = f(\mathbf{z}) + pg(\mathbf{z})$; and $A^{[l+1]}(\mathbf{z},w) = [\partial A^{[l]}(\mathbf{z},u)/\partial \mathbf{z}](f(\mathbf{z}) + pg(\mathbf{z}))\forall l \in N(\text{natural})$

As an example, the second order approximation deduced from this result is given as

$$\begin{aligned}
\mathbf{z}_{k+1} = \mathbf{z}_k + \{f(\mathbf{z}_k) + p_k g(\mathbf{z}_k)\}T + \bigg[\frac{\partial f}{\partial \mathbf{z}}(\mathbf{z}_k)f(\mathbf{z}_k) \\
+ p_k\bigg\{\frac{\partial g}{\partial \mathbf{z}}(\mathbf{z})f(\mathbf{z}_k) + \frac{\partial f}{\partial \mathbf{z}}(\mathbf{z}_k)g(\mathbf{z}_k)\bigg\} + p_k^2\bigg\{\frac{\partial g}{\partial \mathbf{z}}(\mathbf{z})g(\mathbf{z}_k)\bigg\}\bigg] \tag{34}
\end{aligned}$$

Depending on the type and behavior of the nonlinearity, more terms may be added to obtain a more accurate approximate solution. However, if the nonlinear function is not differentiable at a given step then this method cannot be used. For example, if the nonlinearity is modeled as bilinear and not differentiable at a specific point, then this method will result in a nonreliable solution. For the nonlinearity used in this study the Taylor expansion solution is applicable. The outcomes from the two discretization solutions are presented in the "Results" section.

Estimation

Now, the authors provide the methodology for estimating the system state as it evolves over time. With the formulation and variables as defined in the previous sections, the graphical dynamic Bayesian network (DBN) representation of the system evolution is shown in Fig. 1. In sequential BN slices, the system state $\mathbf{z}$ evolves with time based on the input random variables w and $\mathbf{f}$ and the system state at the previous time step. Observations $\mathbf{y}$ (shaded nodes in the DBN) at each time slice are made with some measurement noise $\mathbf{v}$ and
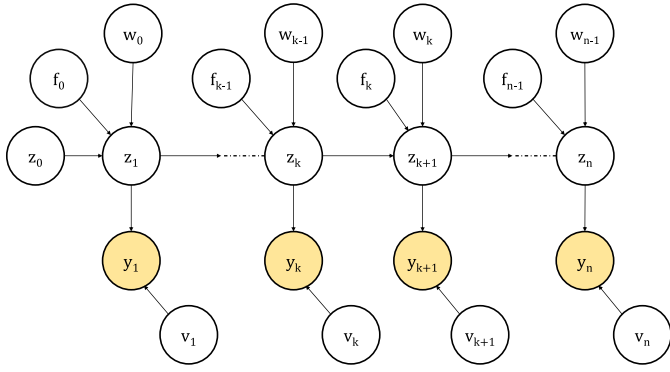
Fig. 1. DBN representation of system evolution

conditioned on the system state. The system is visualized to be Bayesian because the state at a time step is estimated from the previous step and then conditioned using the sensor observation at the given step. Kalman filter frameworks are used to perform the updating.

Observation Equation

Observations used to estimate the maximum response are from structure-mounted accelerometers. The sensors measure the total acceleration of the structure

$$a_t = \ddot{u}_s + 1 a_g \tag{35}$$

Combining with the equation of motion Eq. (1), this can be written as

$$\mathbf{a_t} = -\mathbf{M}^{-1}\mathbf{F}(\mathbf{u_s}) - \mathbf{M}^{-1}\mathbf{C}\dot{\mathbf{u}_s} + \mathbf{M}^{-1}\mathbf{f} \tag{36}$$

Let $\mathbf{S}$ define the matrix that selects the degrees of freedom where accelerometers are placed. The observation equation is then given as

$$\mathbf{y_k} = \mathbf{D}(\mathbf{z_k}) + \mathbf{v_k} + \mathbf{SM}^{-1}\mathbf{f_k} \tag{37}$$

where

$$\mathbf{D} = -\mathbf{SM}^{-1}[\,0 \quad 0 \quad 0 \quad \mathbf{C}\,] - \mathbf{SM}^{-1}\mathbf{F}(\mathbf{u_s}) \tag{38}$$

and v_k = measurement error, which is taken to be normally distributed with zero mean and time-independent variance σ_v^2. The effect of the uncertainty in the sensor measurements on the accuracy of the estimation is investigated in the results section. The random noise $\mathbf{f}$ is modeled as a normally distributed zero-mean process with statistically independent variances for each time step and degree of freedom such that the covariance matrix is given by $\sigma_f^2 \mathbf{I}$. This random term accounts for ambient noise and additional environmental uncertainties.

Extended Kalman Filter

Based on the sensor measurements $\mathbf{y}$, the extended Kalman filter (EKF) can be used to estimate the evolution of the nonlinear system state z. In this study, an overview of EKF is presented. The reader is referred to other texts, (e.g., Terejanu 2008) for further details. The EKF propagates the state space vector by linearizing all nonlinear mappings about the mean of the previous time step. It is then updated using approximate correctors based on the gradients or Jacobians of the mappings. The framework gives the mean vector and covariance matrix for the system state at every time step.

Consider a system with evolution equation

$$\mathbf{z}_{k+1} = f_k(\mathbf{z}_k) + w_k \tag{39}$$

and observation equation

$$\mathbf{y}_{k+1} = h_{k+1}(\mathbf{z}_{k+1}) + v_{k+1} \tag{40}$$

where $f_k(\mathbf{z}_k)$ represents the system evolution as in Eq. (26); and $h_{k+1}(\mathbf{z}_{k+1})$ represents the sensor observation as in Eq. (37). First, the state is predicted based on the expected value of the evolution equation about the mean at the previous time step.

$$\mathbf{z}_{k+1}^p = f(\mathbf{z}_k^F) \tag{41}$$

$$\mathbf{V}_{k+1}^p = Q_k + \nabla f_{k|z_k^F} V_k^F \nabla f_{k|z_k^F}^T \tag{42}$$

where $\mathbf{z}$ and $\mathbf{V}$ represent the mean and variance of a state variable, respectively; superscript p represents values in the predictor phase; F represents final estimated values; and Q_k = variance of input parameter w at time slice t_k.

Next, the estimated value from the predictor phase is corrected through conditioning on the observation matrix. Correction based on the error in the observed value of $\mathbf{y}$ compared to the projected value of $\mathbf{y}$ using the estimated state results in the final estimated mean and variance

$$\mathbf{z}_{k+1}^F = \mathbf{z}_{k+1}^p + \mathbf{V}_{k+1}^p \nabla h_{k+1}^T (\nabla h_{k+1} \mathbf{V}_{k+1}^p \nabla h_{k+1}^T + R_{k+1})^{-1}$$
$$\times (\mathbf{y}_{k+1} - h_{k+1}(\mathbf{z}_{k+1}^p)) \tag{43}$$

$$\mathbf{V}_{k+1}^F = \mathbf{V}_{k+1}^p - \mathbf{V}_{k+1}^p \nabla h_{k+1}^T (R_{k+1} + \nabla h_{k+1} \mathbf{V}_{k+1}^p \nabla h_{k+1}^T)^{-1}$$
$$\times \nabla h_{k+1} \mathbf{V}_{k+1}^p \tag{44}$$

where R = variance with respect to v.

Unscented Kalman Filter

The unscented Kalman filter (UKF) can also be used to infer the state space vector from observations. Theoretically, and as shown in Mariani and Ghisi (2007), it results in more accurate estimates than the EKF for nonlinear problems. The UKF distributes a set of stochastic sigma points for the state vector at each time step and propagates them through the actual nonlinear mapping. The order of accuracy for the mean and covariance obtained through this process depends on the number of sigma points. Sigma points are scattered about the mean of the previous time step and are $2n + 1$ in number, where n is the length of state space vector. The sigma points are weighted such that $\sum_{i=0}^{2n} W = 1$, where W is the weight associated with the ith sigma point.

Values of the sigma points are chosen such that

$$\mathbf{z}_{k-1}^0 = \mathbf{z}_{k-1}^F \tag{45a}$$

$$\mathbf{z}_{k-1}^j = \mathbf{z}_{k-1}^F + \left[\sqrt{(\psi^2 n)\mathbf{V}_{k-1}^F}\right]_j \qquad j \in [1,n] \tag{45b}$$

$$\mathbf{z}_{k-1}^{j+n} = \mathbf{z}_{k-1}^F - \left[\sqrt{(\psi^2 n)\mathbf{V}_{k-1}^F}\right]_j \qquad j \in [1,n] \tag{45c}$$

where the first sigma point is chosen at $\mathbf{z}_{k-1}^F$, the mean of the state vector at the previous time step; $\mathbf{V}_{k-1}^F$ = variance; and ψ^2 = constant defining the distance of a sigma point from the previous mean.

The weight attached to the mean of each sigma point is given as

$$
W_i^m = \begin{cases} \dfrac{\psi^2 - 1}{\psi^2} & i = 0 \\[2ex] \dfrac{1}{2\psi^2 n} & \text{otherwise} \end{cases}
\tag{46}
$$

The weight attached to the variance of each sigma point is

$$
W_i^c = \begin{cases} \dfrac{\psi^2 - 1}{\psi^2} + 3 - \psi^2 & i = 0 \\[2ex] \dfrac{1}{2\psi^2 n} & \text{otherwise} \end{cases}
\tag{47}
$$

In the predictor phase, every sigma point is propagated through the discretization function and the mean and variance of the prediction is calculated using the weights defined in Eqs. (46) and (47). Estimates of the mean and variance in the predictor phase are given as

$$
\mathbf{z}_k^{p,i} = f(\mathbf{z}_{k-1}^i)
\tag{48}
$$

$$
\mathbf{z}_k^p = \sum_{i=0}^{2n} W_i^m \mathbf{z}_k^{p,i}
\tag{49}
$$

$$
\mathbf{V}_k^p = \sum_{i=0}^{2n} W_i^c (z_k^{p,i} - \mathbf{z}_k^p)(\mathbf{z}_k^{p,i} - \mathbf{z}_k^p)^T + Q_{k-1}
\tag{50}
$$

where Q_{k-1} = variance of input parameter w at time slice t_{k-1}.

The predicted values of the mean and variance of the system state are again conditioned using the observation matrix in the corrector phase to produce the final estimated values

$$
\mathbf{z}_k^F = \mathbf{z}_k^p + \mathbf{V}_k^p \nabla h_k^T (\nabla h_k \mathbf{V}_k^p \nabla h_k^T + R_k)^{-1} [\mathbf{y}_k - h(x_k^p)]
\tag{51}
$$

$$
\mathbf{V}_k^F = \mathbf{V}_k^p - \mathbf{V}_k^p \nabla h_k^T (\nabla h_k \mathbf{V}_k^p \nabla h_k^T + R_k)^{-1} \nabla h_{k+1} \mathbf{V}_k^p
\tag{52}
$$

where R = variance with respect to v. Estimation accuracy using EKF compared to UKF is given in the "Results" section.

Authors Distribution of the Maximum Response

The EKF and UKF produce time history estimates of the system state. For reliability problems, the maximum response is of particular interest. To obtain the distribution of the maximum response, the authors use the analytical solution for extreme values of the inferred structural response derived in Tien et al. (2016). This is based on an assumption of exceedances of extreme values over safe thresholds as Poisson events, which holds for high thresholds and low-probability events. Thus, the probability of the response in an interval $[0, T]$ exceeding a given threshold value ζ can be approximated by

$$
P(Z_{\max} > \zeta) = 1 - P(Z_{\max} \leq \zeta) \approx 1 - \exp[-\int_0^T \nu(\zeta^+, t) dt]
\tag{53}
$$

where $Z_{\max} = \max_t[Z(t)]$ is the extreme value for the nonstationary process $Z(t)$, which is a function of the system state $\mathbf{z_s}$. The variable T is the duration of the response and $\nu(\zeta^+, t)$ the mean ζ-level up-crossing rate.

To obtain an expression for $\nu(\zeta^+, t)$, a new process $X(t) = z(t) - \mu_z(t)$ with zero mean and standard deviation $\sigma_X(t) = \sigma_Z(t)$ is defined with an updated threshold for the new process, $\eta(t) = \zeta - |\mu_z(t)|$. In this case, the crossing rate becomes

$$
\nu(\zeta^+, t) = \nu_X[\eta(t)^+, t]
$$

$$
= \frac{\exp(\frac{-1\eta^2}{2\sigma_X^2})}{2\pi\sigma_X\sigma_{\dot{X}}\sqrt{1-\rho^2}} \left\{ \sigma_{\dot{X}}^2(1-\rho^2) \exp\left[-\frac{r^2}{2\sigma_{\dot{X}}^2(1-\rho^2)}\right] \right.
$$
$$
\left. + \sqrt{2\pi(1-\rho^2)}\sigma_{\dot{X}} \left[1 - \Phi\left(\frac{r}{\sigma_{\dot{X}}\sqrt{1-\rho^2}}\right)\right] \left(\frac{\sigma_{\dot{X}}\rho\eta}{\sigma_X} - \dot{\eta}\right) \right\}
\tag{54}
$$

where σ_X and $\sigma_{\dot{X}}$ = standard deviations of the processes X and $\dot{X}$, respectively; $\rho = \rho_{X(t)\dot{X}(t)} = \text{cov}[X(t)\dot{X}(t)]/\sigma_X\sigma_{\dot{X}}$ is the time-dependent correlation coefficient; $r = \dot{\eta} - \sigma_{\dot{X}}\rho\eta/\sigma_X$; and $\Phi(.)$ denotes the normal cumulative distribution function (CDF).

The values in Eq. (54) are obtained from the EKF and UKF inference results. The outcome is the CDF of the exceedance probability of the maximum response at high thresholds. This enables probabilistic assessment of the risk of the structural response exceeding a given threshold over the duration of the excitation, including for small exceedance probabilities that would be infeasible to obtain using alternative sampling-based methods.

Application

Modeling the Structure

The proposed method is applied to a shear-type building of 10 stories as shown in Fig. 2 to demonstrate its use. This model is chosen
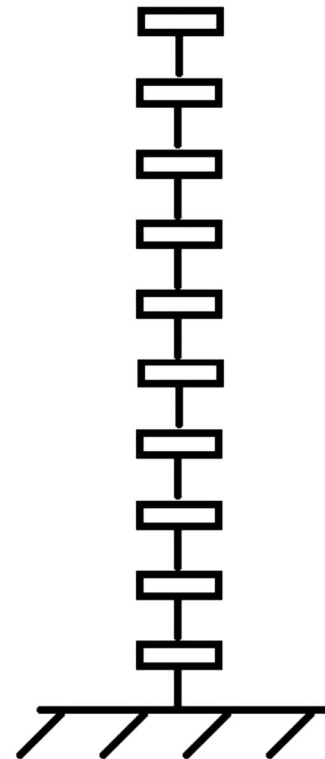

Fig. 2. 10-story shear-type structure

to be consistent with Tien et al. (2016) and facilitate comparison of the results with the linear case. For application to real-world problems, a condensed structural parameter matrix can be used based on predicted eigenvalues of degrees of freedom with uncertainties added to reflect modeling errors. The robustness of the methodology to uncertainty in assumed parameters is investigated later in the study. The stiffness for each story is assumed to follow the Bouc-Wen model, with the resistive force given as $F(t) = \alpha K_i u_s(t) + (1 - \alpha) D K_i \varphi(t)$. In this case α is the ratio of final to initial stiffness K_i and $\varphi(t)$ is a hysteretic parameter given by $\dot{\varphi}(t) = A\dot{u}_s(t) - \beta|\dot{u}_s(t)||\varphi(t)|^{n-1}\varphi(t) - \gamma\dot{u}_s(t)|\varphi(t)|^n$.

For each story, the authors assume the mean values of mass m and stiffness parameter k_i to be unity and damping constant c to be 0.1 such that the coefficient of damping is 5% in the linear case. Variables α, D 1, A, β, γ, and n are chosen to be 0.5, 1, 1, 0.5, −1.5, and 2, respectively, as in Wen (1980). Initial results in the following section assume one known realization of values for the story parameters. To reflect the uncertainty in the ability to know the values of structural parameters exactly, these parameters are later randomized, distributing them with increasing coefficients of variation to investigate the performance of the methodology under increasing degrees of uncertainty.

The ambient noise and sensor measurement error are modeled as zero-mean Gaussian processes, with variances 0.5 and 0.25 m/s^2, respectively, and assuming independence between sensors. One sensor is assumed to be placed on each story. The effect of varying the number, placement, and accuracy of the sensors on the estimation error is presented at the end of the "Results" section. As previously described, the study uses a Bouc-Wen model for the force nonlinearity. However, the results for a cubic or bilinear stiffness model have been found to be qualitatively consistent with the results presented in this study. Finally, it is noted that probabilistic inference on accelerations, velocities, and displacements at all stories can be obtained using the proposed methodology. The results shown are for the interstory drift between stories four and five, called interstory drift #5, throughout this paper for consistency and to demonstrate the ability of the method to estimate interstory drift based on measured accelerations.

Modeling the Ground Excitation

To model the stochastic ground excitation, an earthquake is simulated as proposed by Rezaeian and Der Kiureghian (2010). Acceleration at the bedrock w is modeled as a modulated, band-limited, normally distributed white noise process with zero mean and time-varying variance. The time-dependent variance is treated as proportional to a gamma probability density function (PDF). A scaled gamma PDF is a reasonable representation of an earthquake as it is nonnegative, starts at and tends to zero, and follows the shape of most earthquakes skewed with a longer right-side tail. The shape (k) and scale (θ) parameters for the gamma PDF are found based on the seismic variables as

$$k = \frac{t_{eq}^{max}}{\theta} + 1 \qquad (55)$$

$$\theta = -\frac{1}{2}t_{eq}^{max} + \frac{1}{4}\sqrt{4t_{eq}^{max2} + D_{5-95}^2} \qquad (56)$$

These parameters ensure that the mode of the PDF coincides with the time for the maximum intensity of the earthquake t_{eq}^{max} and the central 90% of the distribution corresponds with the total duration of the earthquake D_{5-95}, which is defined as the time between 5 and 95% Arias intensity values. A representative
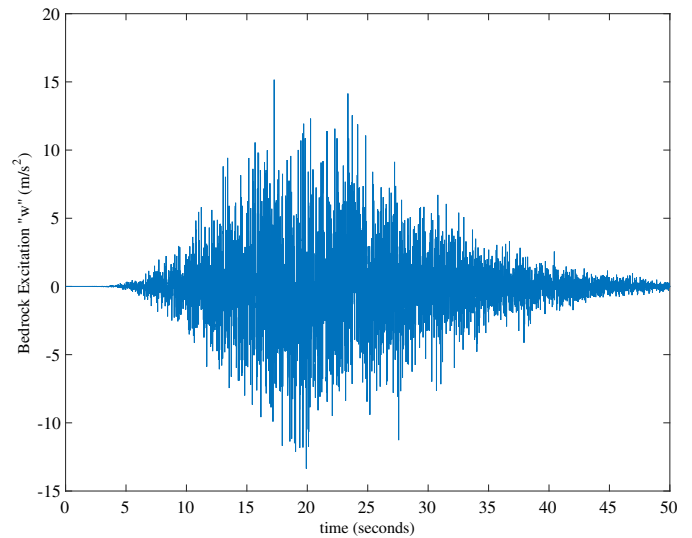

Fig. 3. Sample bedrock excitation w versus time, where w is normally distributed with time-dependent variance proportional to a gamma PDF

simulation of bedrock motion w is shown in Fig. 3 with $t_{eq}^{max} = 20$ s, $D_{5-95} = 25$ s, and scaled by a factor of 70 with discretization time step $= 0.01$ s.

The parameters for the input motion are generally subject to high degrees of uncertainty. In the first part of this study, these values are assumed to be known at the site of interest. Later, the robustness of the proposed method to uncertainty in these input motion parameters is investigated and demonstrated. From the bedrock excitation w, the surface acceleration is calculated using ground filter parameters of $\omega_g/2\pi = 1.5$ and $\xi_g = 0.4$. The effect of uncertainty in ground parameter values is investigated as well.

The randomized earthquake is used to generate an observation matrix for the sensors placed on the structure. These observations are used to estimate the structural response under the excitation. At the same time, the simulation finds the actual response of the structure under the given ground motion. The estimated response using only the information from the sensor measurements is compared with the actual response to examine the accuracy of the method.

Results

The process of investigation is as follows. The authors simulate the bedrock excitation, surface acceleration at the ground, and resulting structural response; this is called the actual response of the system. The structural responses are then used to simulate sensor observations, including measurement error. It is based on these observations that the study estimates the structural response using the DBN formulation and associated EKF and UKF. With the formulation described, the objective is to estimate system state $\mathbf{z}$, including displacement responses, based solely on the accelerometer measurements $\mathbf{y}$. The estimated results are compared with actual responses to assess the performance of the proposed methodology.

The following results are presented: verification of the derived discretization solutions by comparing results using exact versus Taylor approximation methods; comparison of the estimation accuracies using EKF versus UKF; probabilistic inferences on the maximum response of the structure; robustness of the methodology to uncertainties in the structural, ground, and input motion parameters;
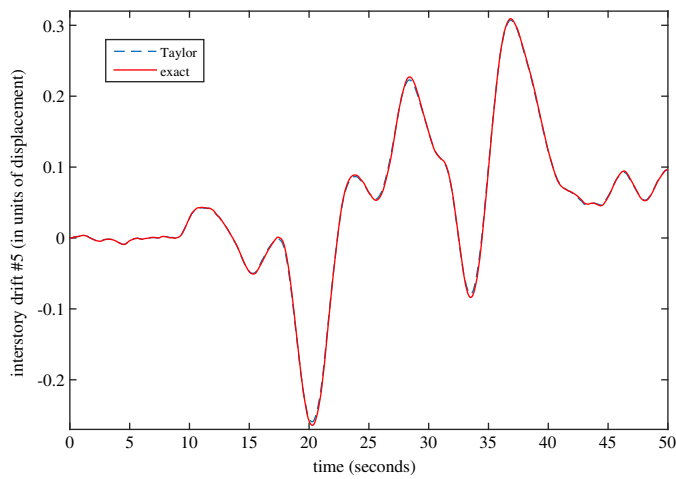
Fig. 4. Interstory drift under input seismic motion for exact and Taylor expansion discretization solutions

Fig. 5. Estimated interstory drift #5 using EKF versus UKF

and the effect of the number, placement, and accuracy of sensors on the ability to estimate the structural response.

Verification of Discretization Formulation

To verify the derivation of the discretization solution for nonlinear systems, the results obtained by the exact solution are compared to the Taylor approximation up to the second derivative term. The simulated ground motion is used as the direct input to compare the resulting responses. Fig. 4 shows the results for the two discretization solutions for the interstory drift between stories four and five. The figure shows a close correspondence between the exact and Taylor discretization solutions, including capturing of the peaks. Including more terms in the Taylor formulation will decrease the error even further. However, it will increase the computational time and in some cases may not be feasible if the nonlinear function is nondifferentiable. The approximate solution will also contain more error with increasing nonlinearity. The exact discretization formulation is therefore used in the remaining portions of this study.

EKF versus UKF

Fig. 5 shows the estimation results using UKF and EKF compared with the actual response from the simulation for the interstory drift between floors four and five. To facilitate direct comparison between UKF and EKF, this analysis assumes data is available from accelerometers mounted at all 10 degrees of freedom. The results are shown more clearly in Fig. 6, which focuses on the highest peak near 37 s to distinguish the plots. From Fig. 6, using the UKF results in a smaller variance in the estimation compared to the EKF, with a narrower band in the UKF $\mu \pm 2\sigma$ estimates. Additionally, the UKF mean estimate corresponds more closely with the actual response. The total root mean square (RMS) error over the full time history with respect to the actual simulation is 0.0073 (in units of displacement) for UKF compared to 0.0091 (in units of displacement) for EKF. Hence, UKF gives a more accurate estimation with lesser variance, and is the preferable framework for use in estimation for this application. Hereafter, estimation results presented are from the UKF.

Note that small deviations in the UKF estimates compared to the actual response are shown in Fig. 5 at the beginning of the time history. This is due to the assumption in the estimation of the variance
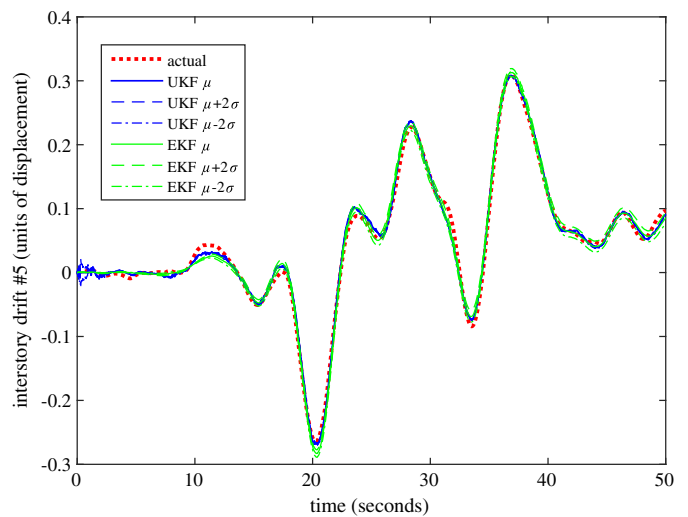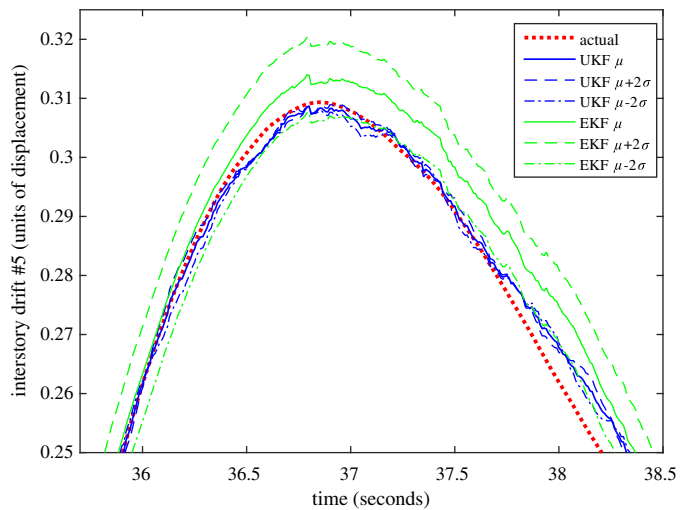

Fig. 6. EKF and UKF estimates at the peak

of the displacement at the initial time step as one unit. However, as evident from Fig. 5 and for the peak in Fig. 6, the estimation variance as the excitation continues is on the order of 10^{-4} (in units of displacement-squared). Thus, while the UKF analysis fluctuates in the beginning of the time history, it quickly converges to the actual response. As the variance of the displacement would not be known beforehand, the initial assumption is not changed.

Distribution of the Maximum Response

The ability to use the time history estimates as previously shown to perform probabilistic inference on the maximum response is now investigated. The results from the analytical formulation for probability of exceedance of the process above safe thresholds are compared with Monte Carlo (MC) simulations. A total of 10,000 MC realizations are generated for the posterior process with randomly sampled priors.

Fig. 7 shows the obtained stochastic distribution of the maximum response. It gives the complementary CDF of the maximum interstory drift of each story, i.e., the probability of the maximum
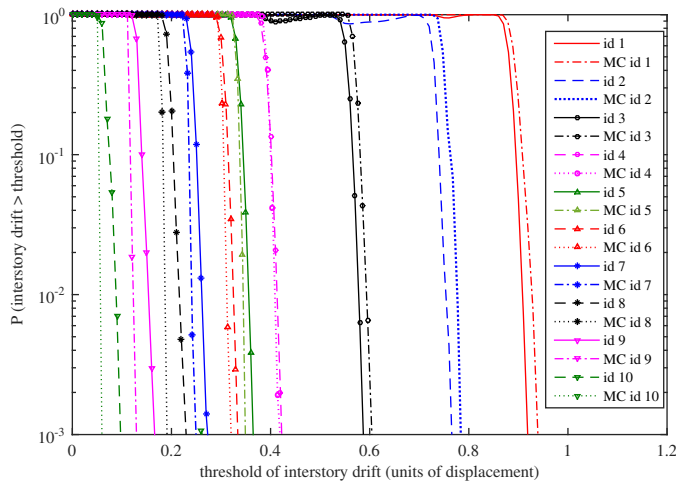
Fig. 7. Analytical and MC distributions of maximum response with respect to various displacement thresholds

response exceeding a threshold value of displacement. For each story, the analytical solutions, e.g., id 1 for interstory drift at the first floor, are compared with MC realizations, e.g., MC id 1. The distribution for MC is the empirical complementary CDF obtained by counting the number of simulations where the absolute maxima exceeds a threshold out of the total 10,000 MC simulations.

In Fig. 7, there is close correspondence between the analytical and MC results across the degrees of freedom. This shows the ability of the formulation to obtain stochastic distributions of the maximum response based on the sensor measurement data. However, the analytical solution plots display some fluctuations at lower thresholds as can be seen in the plots for id 1, id 2, and id 3 in Fig. 7. This is in contrast to the expected monotonically decreasing complementary CDF. This is because of the assumption of Poisson crossings above the threshold of interest. For example, at low thresholds, the assumption does not hold as clusters of crossings are likely. Therefore, the analytical solution is suitable for use as a predictor at high thresholds and low probabilities of exceedance. These are the significant, high-impact events that are of interest, particularly when the structure is designed to withstand lower threshold displacements. The formulation presented enables risk analysis results

for these extreme events, which may be infeasible to obtain using MC approaches.

Robustness of Methodology to Uncertainty in Structural and Ground Parameters

The analyses up to this point have been based on the assumption that all system parameters are known. In general, these parameters are estimated and subject to varying degrees of uncertainty. Instead of the previously assumed single values for each parameter, in this section they are randomized with increasing coefficients of variation. For structural parameters, damping is in general more difficult to estimate compared to mass and stiffness. Therefore, varying coefficients of variation (COVs) of 0–20% from the nominal values for mass and stiffness and 0–40% for damping are used. The values of these parameters are lognormally distributed at each level of COV. Similarly, the ground parameters are also uncertain. The nominal values of ground parameters are set as assumed previously with $\omega_g/2\pi = 1.5$ and $\xi_g = 0.4$. These parameters are now varied by distributing them lognormally with COVs ranging from 0 to 20%.

The combined effect of uncertainty in structural and ground parameters is analyzed. For consistency, the estimation result for the interstory drift between stories four and five are analyzed. Fig. 8(a) shows the RMS error of the estimated compared to the actual response with a point plotted for each value of COV in increments of 1% (2% for damping). For Fig. 8(a), 20 samples are simulated for each COV value and the mean and standard deviation of RMS error is calculated over all samples.

From Fig. 8(a), the mean RMS error remains nearly constant over the range of COVs, while the standard deviation increases with increasing COVs. Noting the ordinate scale, the maximum $\mu + 2\sigma$ value of RMS error is less than 5.5% of the maximum response, at 20% COV for mass, stiffness, ground parameters, and 40% COV for damping. Thus, the inference is robust to uncertainty in the structural and ground parameters even in the nonlinear case. This is because the UKF is able to use the information from sensor measurements to overcome the effect of the parameter uncertainty. It adapts to the discrepancies in the parameters through the changing observation matrix at each time step.

The variation of the estimate of the maximum structural response as a function of varying parameters is also of interest. Fig. 8(b) depicts the actual absolute maximum of the structural response with randomly distributed parameters compared to UKF
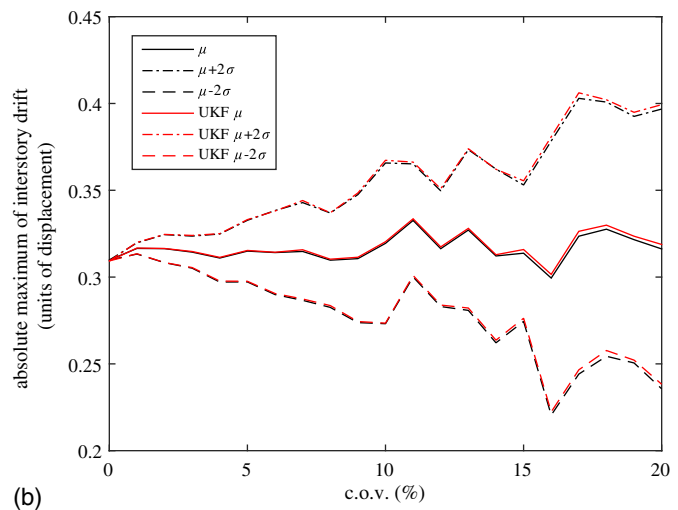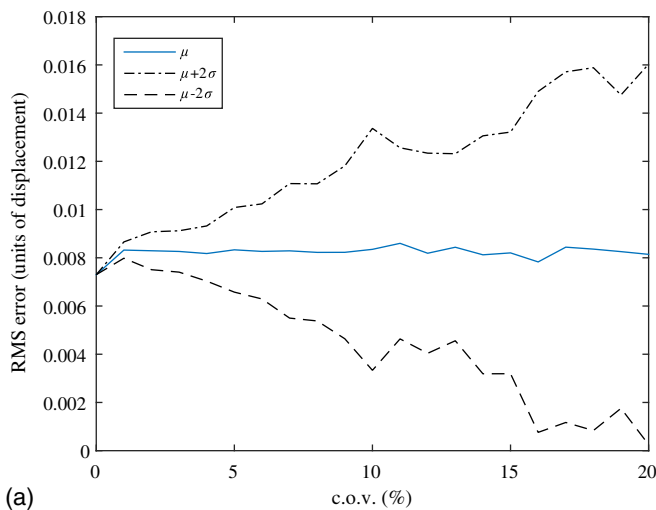

Fig. 8. (a) RMS error and (b) maximum response as a function of increasing COVs of structural and ground parameters
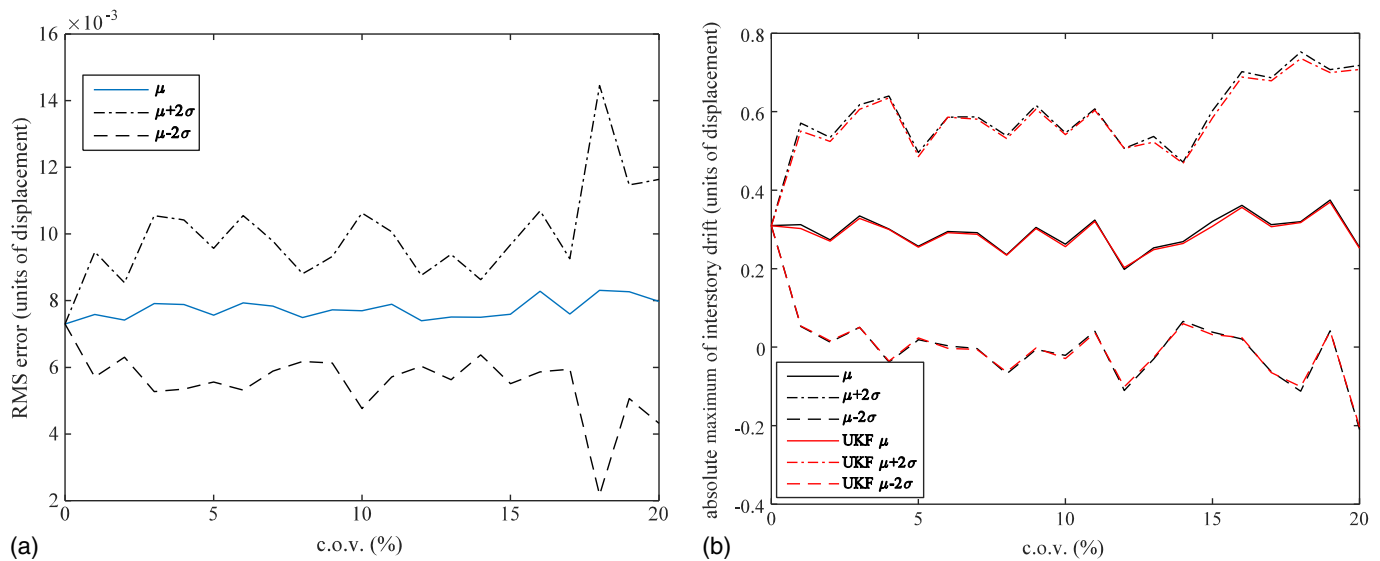
Fig. 9. (a) RMS error; (b) estimated maximum response as a function of increasing COVs of input motion parameters

estimates based on nominal values of the parameters. Coefficients of variation are again increasing from 0 to 20% with COV of the damping coefficient being twice that of the other parameters.

From Fig. 8(b), the UKF-estimated mean maximum structural response stays within 0.003 units, or within less than 1%, of the actual maximum response even as COV increases from 0 to 20% for mass, stiffness, and ground parameters and 0 to 40% for damping. In addition, the variation of the estimate over 20 samples remains consistent with the variation of the actual response as COV increases. Results were similar in looking at structural and ground parameters separately. Thus, the estimate of the maximum is robust to uncertainty in the assumed parameters for the methodology.

Robustness of Methodology to Uncertainty in Input Motion Parameters

The input motion parameters to describe an earthquake excitation are highly variable and generally unknown. The input motions are recorded and the parameters later investigated. However, this study uses a simulated ground motion and hence it is possible to analyze the robustness of the methodology to varying input motion parameters. Note that input motion uncertainty is analyzed separately because while variations in structural and ground parameters reflect uncertainty in assumptions for the analysis, variations in input parameters reflect performance of the methodology under different earthquake events.

In the stochastic ground motion model, two parameters are used to define the earthquake: time of maximum intensity $t_{eq}^{\max}$, and effective duration of the earthquake between 5 and 95% of the Arias intensity values D_{5-95}. In this case, these parameters are varied normally with COVs ranging between 0 and 20% to reflect variability across earthquake motions. Fig. 9(a) shows the performance of the method for COVs varying in increments of 1%, with the RMS error again calculated as the mean of 20 simulations at every value of COV.

From Fig. 9(a), the RMS error with varying input parameters remains nearly constant for all simulations, both in terms of the mean and standard deviation. This is because the evolution of the system per the UKF formulation in Eq. (51) depends only on the structural and ground parameters, without input parameters.
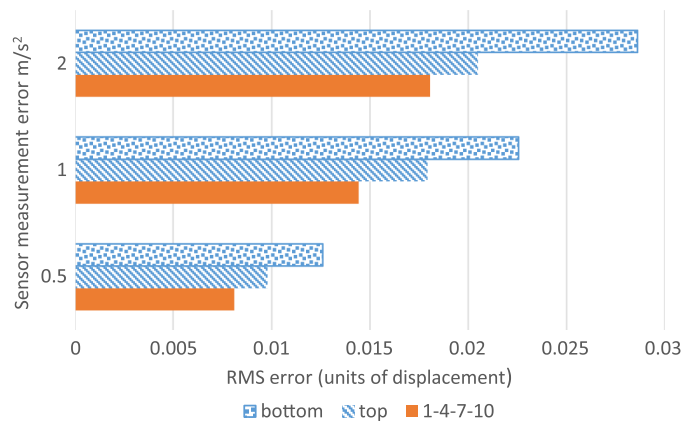

Fig. 10. RMS errors for varying sensor configurations in terms of number, placement, and precision

Fig. 9(b) shows the behavior of the maximum response with increasing variation in input motion parameters. In all cases, the estimated response, both in terms of mean and standard deviation, follows closely the actual maximum response. This demonstrates the estimation methodology to be robust to uncertainty in the input motion.

Varying Measurement Characteristics

Finally, the effect of the number, placement positions, and measurement errors of the sensors is investigated. Fig. 10 shows RMS error results for three different sensor configurations. First, when one sensor is placed at the bottom floor; second, when one sensor is placed at the top floor; and third, when four sensors are placed throughout the structure on Floors 1, 4, 7, and 10. The sensor measurement error is also varied as 0.5, 1, and 2 m/s². From Fig. 10, as expected, the RMS error is the lowest when more sensors are used because more information is available on which to condition the estimation. The RMS error is the highest when only one sensor is placed at the bottom floor because this captures the smallest response, thereby providing the least amount of

information. Consistent with previous results in Tien et al. (2013, 2016) when only one sensor is placed on the structure, it is advantageous to mount it on the top floor compared to the bottom floor.

As expected, looking at sensor noise, the error in the estimates increases with increasing uncertainty in the sensor measurements. From Fig. 10, a tradeoff between the number of sensors and the measurement error is observed. For comparable estimation accuracy, more sensors should be used if the sensor measurement error is higher, but with better precision sensors, fewer sensors can be used. However, the difference between placing a sensor at the top compared to the bottom of the structure is most significant. These results can be applied to structural health monitoring systems, in designing effective instrumentation configurations to best support the estimation of structural response.

Conclusion

The proposed methodology uses the Kalman-estimated system state to assess the nonlinear response of a structure under seismic load based on observations from accelerometers placed on the structure. The methodology includes an exact discretization solution derived for the nonlinear system and validated against a Taylor expansion-based discretization method. The estimation results show the UKF to provide the most accurate estimations of structural response, particularly at the peak. The methodology provides a probabilistic assessment of the distribution of the maximum response in particular, with the analytical results verified through comparison with MC simulations. Through analyses of the impact of variations in the system parameters on the results, the methodology is shown to be robust to inaccurate or uncertain assumptions for the structural and ground parameters, as well as across input motions. Additionally, inferences drawn support decision making in structural health monitoring applications, including in the number, placement, and accuracy of sensors required to assess structural response. The probabilistic formulation presented enables estimation of the stochastic distribution of the maximum nonlinear response, under conditions of uncertainty for the system, excitation, and measurement parameters.

References

Al-Hussein, A., and Haldar, A. (2015). "Novel unscented Kalman filter for health assessment of structural systems with unknown input." *J. Eng. Mech.*, 10.1061/(ASCE)EM.1943-7889.0000926, 04015012.

Au, S. K., Zhang, F. L., and Ni, Y. C. (2013). "Bayesian operational modal analysis: Theory, computation, practice." *Comp. Struct.*, 126, 3–14.

Barber, D. (2012). *Bayesian reasoning and machine learning*, Cambridge University Press, Cambridge, U.K.

Bouc, R. (1967). "Forced vibration of mechanical systems with hysteresis." *Proc., 4th Conf. on Nonlinear Oscillation*, Prague, Czech Republic, 315.

Chatzi, E. N., and Smyth, A. W. (2009). "The unscented Kalman filter and particle filter methods for nonlinear structural system identification with non-collocated heterogeneous sensing." *J. Struct. Control Health Monit*, 16(1), 99–123.

Foun, K. (2010). "Identification of civil structural parameters using the extended Kalman filter." Master's thesis, Massachusetts Institute of Technology, Cambridge, MA.

Guy, J. (2006). "Lagrange characteristic method for solving a class of nonlinear partial differential equations of fractional order." *Appl. Math. Letters*, 19(9), 873—880.

Hori, N., Mori, T., and Nikiforuk, P. N. (1992). "A new perspective for discrete-time models of a continuous-time system." *IEEE Trans. Autom. Control*, 37(7), 1013–1017.

Hoshiya, M., and Saito, E. (1984). "Structural identification by extended Kalman filter." *J. Eng. Mech.*, 10.1061/(ASCE)0733-9399(1984) 110:12(1757), 1757–1770.

Hurtado, J. E., and Barbat, A. H. (1996). "Improved stochastic linearization method using mixed distributions." *Struct. Saf.*, 18(1), 49–62.

Ikhouane, F., Mañosa, V., and Rodellar, J. (2007). "Dynamic properties of the hysteretic Bouc-Wen model." *Syst. Control Letters*, 56(3), 197–205.

Jeen-Shang, L., and Yigong, Z. (1994). "Nonlinear structural identification using extended Kalman filter." *Comput. Struct.*, 52(4), 757–764.

Kalman, R. E. (1960). "A new approach to linear filtering and prediction problems." *J. Basic Eng.*, 82(1), 35–45.

Katafygiotis, L. S., and Yuen, K. V. (2001). "Bayesian spectral density approach for modal updating using ambient data." *Earthquake Eng. Struct. Dyn.*, 30(8), 1103–1123.

Kazantzis, N., and Kravaris, C. (1999). "Time-discretization of nonlinear control systems via Taylor methods." *Computers Chem. Eng.*, 23(6), 763–784.

Mariani, S., and Ghisi, A. (2007). "Unscented Kalman filtering for nonlinear structural dynamics." *Nonlinear Dyn (2007)*, 49(1–2), 131–150.

Markazi, A. H. D., and Hori, N. (1995). "Discretization of continuous-time control systems with guaranteed stability." *IEE Control Theory Appl.*, 142(4), 323–328.

Mu, H. Q., and Yuen, K. V. (2015). "Novel outlier-resistant extended Kalman filter for robust online structural identification." *J. Eng. Mech.*, 10.1061/(ASCE)EM.1943-7889.0000810, 04014100.

Murphy, K. (2002). "Dynamic Bayesian networks: Representation, inference and learning." Ph.D. thesis, Univ. of California, Berkeley, CA.

Murphy, K. (2012). *Machine learning: A probabilistic perspective*, MIT Press, Cambridge, MA.

Nesic, D., and Teel, A. (2004). "A framework for stabilization of nonlinear sampled-data systems based on their approximate discrete-time models." *IEEE Trans. Autom. Control*, 49(7), 1103–1122.

Rezaeian, S., and Der Kiureghian, A. (2010). "Stochastic modeling and simulation of ground motions for performance based earthquake engineering." *Rep. No. 2010/02*, Pacific Earthquake Engineering Research Center, Univ. of California, Berkeley, CA.

Rice, S. O. (1944). "Mathematical analysis of random noise." *Bell Syst. Tech. J.*, 23(3), 282–332.

Sakamoto, T., Hori, N., and Ochi, Y. (2011). "Exact linearization and discretization of nonlinear systems satisfying a Lagrange PDE condition." *Trans. Canadian Soc. Mech. Eng.*, 35(2), 215–228.

Song, J., and Der Kiureghian, A. (2006). "Generalized Bouc-Wen model for highly asymmetric hysteresis." *J. Eng. Mech.*, 132(6), 610–618.

Terejanu, G. A. (2008). "Extended Kalman filter tutorial." Univ. at Buffalo, Buffalo, NY.

Tien, I. (2014). "Bayesian network methods for modeling and reliability assessment of infrastructure systems." Ph.D. thesis, Univ. of California, Berkeley, CA.

Tien, I., Pozzi, M., and Der Kiureghian, A. (2013). "Inference on maximum structural response based on measured accelerations using dynamic Bayesian network." *Safety, reliability, risk and life-cycle performance of structures and infrastructure*, Deodatis G., Ellingwood B., and Frangopol D., eds., CRC Press, New York.

Tien, I., Pozzi, M., and Der Kiureghian, A. (2016). "Probabilistic framework for assessing maximum structural response based on sensor measurements." *Struct. Saf.*, 61, 43–56.

Vanik, M. W., and Beck, J. L. (1997). "A Bayesian probabilistic approach to structural health monitoring." *Technical Rep., EERL 97-07*, California Institute of Technology, Pasadena, CA.

Vanik, M. W., Beck, J. L., and Au, S. K. (2000). "Bayesian probabilistic approach to structural health monitoring." *J. Eng. Mech.*, 10.1061 /(ASCE)0733-9399(2000)126:7(738), 738–745.

Wen, Y. K. (1976). "Method for random vibration of hysteretic systems." *J. Eng. Mech. Div.–Civ. Eng.*, 102(2), 249–263.

Wen, Y. K. (1980). "Equivalent linearization for hysteretic systems under random excitation." *Trans. ASME*, 47(1), 150–154.

Wen, Y. K. (1989). "Methods of random vibration for inelastic structures." *Appl. Mech. Rev.*, 42(2), 39–52.

Wu, M., and Smith, A. W. (2007). "Application of unscented Kalman filter for real-time nonlinear structural system identification." *Struct. Control Health Monit.*, 14(7), 971–990.

Xie, Z., and Feng, J. (2012). "Real-time nonlinear structural system identification via iterated unscented Kalman filter." *Mech. Syst. Signal Processing*, 28, 309–322.

Yang, J. N., Lin, S., Huang, H., and Zhou, L. (2006). "An adaptive extended Kalman filter for structural damage identification." *Struct. Control Health Monit.*, 13(4), 849–867.

Yang, J. N., Pan, S., and Huang, H. (2007). "An adaptive extended Kalman filter for structural damage identification. II: Unknown inputs." *Struct. Control Health Monit.*, 14(3), 497–521.

Yuen, K. V., and Katafygiotis, L. S. (2002). "Bayesian modal updating using complete input and incomplete response noisy measurements." *J. Eng. Mech.*, 10.1061/(ASCE)0733-9399(2002)128:3(340), 340–350.

Zhang, F., and Au, S. (2015). "Probabilistic model for modal properties based on operational modal analysis." *ASCE-ASME J. Risk Uncertainty Eng. Syst., Part A: Civ. Eng.*, 2(3), B4015005.

Zhang, Y., and Chong, K. T. (2006). "Discretization of nonlinear systems with delayed multi-input via Taylor series and scaling and squaring technique." *SICE-ICASE Int. Joint Conf.*, IEEE, New York, 863–860.

Zhang, Y., Kostyukova, O., and Chong, K. T. (2011). "A new time-discretization for delay multiple-input nonlinear systems using the Taylor method and first order hold." *Discrete Appl. Math.*, 159(9), 924–938.

Zheng, Z., Baek, S. J., Yu, D. H., and Chong, K. T. (2013). "Comparison study of the Taylor series based discretization method for nonlinear input-delay systems." *Control Conf. (AUCC)*, IEEE, New York.